Chemical Geology 457 (2017) 149–161

Contents lists available at ScienceDirect

Chemical Geology

journal homepage: www.elsevier.com/locate/chemgeo

Invited research article

Redox properties of clay-rich sediments as assessed by mediated electrochemical analysis: Separating pyrite, siderite and structural Fe in clay minerals

Alwina L. Hoving[a,*], Michael Sander[b], Christophe Bruggeman[c], Thilo Behrends[a]

[a] Department of Earth Sciences - Geochemistry, Faculty of Geosciences, Utrecht University, Princetonplein 9, 3584 CC Utrecht, The Netherlands
[b] Institute of Biogeochemistry and Pollutant Dynamics (IBP), Department of Environmental Systems Science, ETH Zürich, 8092 Zürich, Switzerland
[c] Waste & Disposal Expert Group, Unit R & D Disposal, Belgian Nuclear Research Centre (SCK•CEN), Boeretang 200, Mol, Belgium

ARTICLE INFO

Keywords:
Redox properties
Electrochemistry
Clay minerals
Pyrite
Siderite
Boom Clay

ABSTRACT

Redox reactions with Fe-containing minerals in clay-rich sediments largely affect the speciation, mobility, and (bio-) availability of redox-sensitive contaminants. Here, we use mediated electrochemical oxidation (MEO) and reduction (MER), to quantify the electron accepting and donating capacities (EAC and EDC) of Boom Clay, a potential host formation for radioactive waste disposal. The relevant redox-active minerals pyrite, siderite, smectite and illite were first studied separately. MEO and MER of smectites and illites resulted in sharp current peak responses, reflecting fast electron transfer kinetics. Conversely, broad current peaks were obtained from MEO of pyrite. The current response to MEO of siderite was very small. Under the applied electrochemical conditions in MEO, pyrite was not completely oxidized and only a marginal fraction of siderite was oxidized. All structural Fe (Fe_{struct}) in smectites SWa-1 and SWy-1 was redox-active in MER and MEO, whereas in Fithian Illite and IMt-1 only 12–22% of the total Fe_{struct} was available. An empirical equation was used to describe the current curves of the tested minerals. This equation allowed to delineate the relative contributions of these minerals to MEO of their mixtures. The EDC of Boom Clay determined by MEO was 0.2 ± 0.05 mmol e^-/g and predominantly consisted of contributions of pyrite, Fe_{struct} in clays and natural organic matter (NOM). Applying the empirical equation allowed to separate the oxidative current response into the contribution of pyrite with slower oxidation kinetics and the combined contribution of faster reacting Fe_{struct} and natural organic matter (NOM). Due to the absence of NOM isolates from Boom Clay, the EDC of NOM was estimated based on MEO measurements of dissolved organic matter in Boom Clay pore water and the organic carbon content of Boom Clay. The EDC of Fe_{struct} in clays was then obtained by subtracting the contributions of NOM and pyrite from the measured EDC. About 14% of the measured EDC can be attributed to Fe_{struct} which implies that about 50% of the structural Fe^{II} in Boom Clay is redox-active. In contrast, EAC measurements indicate that Fe^{III}_{struct} in Boom Clay is electrochemically inactive.

1. Introduction

The fate and transport of redox sensitive heavy metals, metalloids, and radionuclides in natural and engineered systems are highly dependent on the prevailing redox conditions. Changes in the redox states and hence the speciation of these elements strongly affect solubility, sorption, bioavailability and toxicity (Appelo and Postma, 2005; Borch et al., 2009; Langmuir, 1997; Van der Perk, 2006). Clay-rich sediments are considered as natural barriers for landfills (Parker and Rae, 1998) and as potential host rocks for radioactive waste repositories (Higgo, 1987; IAEA, 2013, 2003; Lee and Tank, 1985). The function of these barriers is to contain potentially hazardous elements by retarding their migration over sufficient long periods and thereby protecting neighboring groundwater bodies and the biosphere. Clay-rich sediments are suitable barriers by suppressing convective transport of solutes due to their low hydraulic conductivity and by their capability to retard transport by interactions between solutes and the solid phase (Higgo, 1987). The latter includes redox reactions: for example reduction of U^{VI} to U^{IV} or of Se^{IV} to Se^0, can lead to an effective immobilization of these elements by forming solids with low solubilities (Breynaert et al., 2010; Bruggeman et al., 2005; Bruggeman and Maes, 2010; Delécaut, 2004). In order to assess the extent to which clay constituents undergo electron transfer reactions with redox-active contaminants, it is critical to have information on the capacities of

* Corresponding author.
E-mail address: A.L.Hoving@uu.nl (A.L. Hoving).

http://dx.doi.org/10.1016/j.chemgeo.2017.03.022
Received 16 January 2017; Received in revised form 21 March 2017; Accepted 23 March 2017
Available online 23 March 2017
0009-2541/

the clay-rich sediment to accept and donate electrons. Here, we investigate the applicability of mediated electrochemical analyses to quantify the electron donating and accepting capacities of clay-rich sediments in the context of geological disposal of radioactive waste (RW).

For RW disposal, clay-rich sediments and rocks are investigated as potential host formations for accommodating a RW repository. These formations include Opalinus Clay in Switzerland, Callovo-Oxfordian Clay in France and Boom Clay in Belgium and the Netherlands (Grambow, 2016). The redox properties of these clay materials have been investigated in numerous studies (De Craen et al., 2004; Gaucher et al., 2004; Wersin et al., 2011). In this work we will investigate Boom Clay (here collectively referring to the Boom Clay Formation in Belgium and the Rupel Clay member in the Netherlands) as a model for argillaceous formations. Boom Clay contains a variety of potentially redox-active solids. Among these, pyrite is generally considered to be the most important phase regarding the reduction and immobilization of redox-active elements such as Se and U (Breynaert et al., 2010; Bruggeman et al., 2005; Bruggeman and Maes, 2010; Delécaut, 2004). However, other redox-active minerals present in the Boom Clay, including natural organic matter (Bruggeman et al., 2007), siderite (Badaut et al., 2012; Scheinost and Charlet, 2008) and clay minerals (Charlet et al., 2007; Jaisi et al., 2009), may also contribute significantly to redox capacities of the clay material and thus to electron exchange reactions with radionuclides.

Reduction and oxidation capacities of sediments, from here on referred to as electron donating and accepting capacities (EDC and EAC), respectively, are often quantified by reacting them with strong chemical oxidants or reductants and monitoring their consumption (Bauer et al., 2007; Heron et al., 1994; Heron and Christensen, 1995; Pedersen et al., 1991). However, these methods may not always measure the relevant capacities for redox reactions with radionuclides because of the aggressive treatments applied. For instance, these conditions may cause minerals to dissolve or change their properties and as a consequence electron accepting and donating capacities may become available that were unavailable in the natural sample prior to harsh treatments. By comparison, mediated electrochemical analysis allows monitoring oxidation and reduction of a solid sample over time under well-defined solution conditions. This is achieved by measuring reductive and oxidative currents that result from the addition of the samples to electrochemical cells that are polarized to stable potentials. The approach relies on the use of dissolved electron transfer mediators to facilitate electron transfer and redox equilibration between the added redox-active solid and the surface of the working electrode (Sander et al., 2015). Integration of the oxidative and reductive current peaks that result from sample addition directly yields the number of electrons exchanged and, when normalized the mass of the analyzed sample, the EDC and EAC values at a specific redox potential. Mediated electrochemical oxidation/reduction (MEO/MER) has already been successfully used on solid suspensions of several smectites (Gorski et al., 2013, 2012a, 2012b, 2011), dissolved organic matter (e.g. Aeschbacher et al., 2012, 2011, 2010; Klüpfel et al., 2014) and Fe (oxyhydr)oxides (Klein et al., 2014). Furthermore, it was recently demonstrated that MER and MEO can be used to quantify electron transfer to and from natural organic matter and iron(III) phases (Lau et al., 2015) in fresh-water and lake sediments and to provide a more holistic picture of electron fluxes in lake sediments with alternating redox conditions (Lau et al., 2016).

The goal of this study was to use mediated electrochemical analyses to quantify the redox capacities of a natural clay-rich sediment and to assess whether the contributions from different dissolved and solid-phase redox-active species could be delineated. To address the latter question, we focused on differences in reaction kinetics during MEO of the various reductants present in Boom Clay. The redox analysis in this work focused on MEO and less on MER, given that Boom Clay is a reduced sediment and primarily contains reduced constituents. Due to the lack of published data on the electro-activity of pyrite, siderite and the clay mineral illite in MEO, we first separately investigated the oxidative current responses of reference standards of these minerals. Based on the results, an empirical equation was developed and parameterized to describe the current response for each reduced mineral in MEO. Besides pure mineral samples, synthetic mixtures of known amounts of pyrite and clay minerals, and siderite and clay minerals were analyzed to validate the empirical model. This parameterized model is then used for the deconvolution of the overall Boom Clay current signal into the separate mineral contributions.

2. Materials and methods

All electrochemical analyses were carried out in an anaerobic glovebox with an argon atmosphere (< 0.1 ppm O_2). Solutions used inside the glovebox were purged with argon for about 4 h before transferring them into the glovebox. All chemicals were purchased from Sigma-Aldrich, except for triquat (1,1-trimethylene 2,2-bipyridyl dibromide) which was synthesized as described by Gorski et al. (2012a).

2.1. Materials

Boom Clay sediment (Belgium classification, which roughly corresponds to Rupel Clay Member of the Rupel Formation in the Dutch classification system) is a marine sediment deposited during the Oligocene (Aertsens et al., 2004; Griffioen et al., 2016). Samples were retrieved from a core collected in Zeeland, the Netherlands, at a depth of 57.76 m (core KB104, slice 24). More information about location, storage and treatments of the core can be found in Behrends et al. (2016). Slicing of the core was performed in a glovebox with N_2/H_2 95%/5% atmosphere to avoid oxidation of redox sensitive material by oxygen. Any further manipulations of the material and experiments were performed inside a glovebox under argon atmosphere. Before electrochemical analysis, the sample was suspended in ultra-high purity water (UHQ, 18.2 MΩ cm, Purelab Ultra, Elga). The solid phase concentration of the suspension was determined by weighing aliquots after drying them inside the glove box. Boom Clay pore water extracted from piezometers, SPRING116 and EG/BS, located in the HADES underground research facility in the Boom Clay in Belgium (Bleyen et al., 2016; De Craen et al., 2004) was sampled by SCK-CEN (Belgian Nuclear Research Centre) and sent in crimp flasks under anaerobic atmosphere.

Four reference clay minerals were used for electrochemical characterization: a ferruginous smectite SWa-1 (Grant County, Washington, USA), montmorillonite SWy-1 (Crook County, Wyoming, USA) and a Cambrian shale illite IMt-1 (Silver Hill, Montana, USA) obtained from the Clay Minerals Society (Chantilly, VA, USA), and the Fithian gray shale illite (Illinois, USA) obtained from Ward's Natural Science Establishment (Rochester, New York). The clay minerals were purified, size-fractionated and Na^+-saturated before analyzing them in the electrochemical set-up. The procedures of these treatments are briefly described hereafter. Natural clay samples can contain a variety of iron minerals such as jarosite and poorly crystalline Fe(oxyhydr)oxides (Anderson and Jenne, 1970; Seabaugh et al., 2006). To remove these potentially present secondary Fe minerals, 1 M HCl was added in a solid to liquid ratio of 1 g: 40 mL. The suspension was then left on a shaking table for 4 h (Claff et al., 2010). The acidic suspensions were subsequently centrifuged (8 min at 3000*g*, SL40R, Thermo Scientific), the supernatants discarded, and the remaining solids were washed three times with 0.1 M HCl by repeated resuspension and centrifugation. The finest size-fraction was separated after re-suspending the remaining solid in UHQ-water and then treating it in an ultrasonic bath for 10 min to de-flocculate the clay minerals. The suspension was then centrifuged at 215*g* for 2 min to isolate particles smaller than 2 μm which remained in the supernatant. The supernatant was decanted and saved. The size-fractionation procedure was repeated until the supernatant was clear

after centrifugation. Afterwards, all supernatants, containing the < 2 μm size fractions, were combined and saved, while the > 2 μm size fraction was discarded.

The reference clay minerals were in an oxidized state when received. To use MEO and determine the EDC of the reduced form of these clay minerals, we chemically reduced aliquots of the < 2 μm clay mineral suspension by a citrate/bicarbonate/dithionite (CBD) reagent (Claff et al., 2010; Gorski et al., 2012a). The dithionite treatment probably did not reflect reduction by naturally occurring reductants or bacteria since irreversible structural alterations could occur upon dithionite reduction that do not occur for example by microbial reduction (e.g. Gorski et al., 2013; Ribeiro et al., 2009; Stucki, 2011). Hence, dithionite reduction provides an upper estimate of the redox sensitive structural Fe^{III} in clay minerals. Here, the dithionite reduction was conducted to test whether reduced Fe in clay minerals was quantifiable by mediated electrochemical oxidation and was not used to mimic natural reduction of clay minerals. The dithionite treatment would also remove any potentially present crystalline iron (oxyhydr) oxides: the CDB reagents were added to the clay suspension in a ratio of 2 g sodium dithionite and 44 mL citrated-bicarbonate buffer (pH 7.5, 0.17 M citrate, 0.11 M bicarbonate) per 1 g clay. After 24 h of reaction time, the supernatant was removed by centrifugation and the residual was washed three times using 1 M deoxygenated $NaClO_4$ by repeated resuspension and centrifugation.

To ensure that both the oxidized and chemically reduced clay minerals were Na^+-saturated, fresh anoxic 1 M $NaClO_4$ was added to both mineral suspensions. After addition, the suspensions were stirred for about 3 h and then left to settle for a day. The supernatant was decanted after which fresh anoxic 1 M $NaClO_4$ was re-added. This saturation process was repeated two more times. The final purified suspensions of the various clay minerals contained between 7 and 15 g/L of suspended solids.

The pyrite sample used for the electrochemical analyses was obtained from Ward's Natural Science Establishment and originated from Zacatecas, Mexico (cubes, hydrothermal). To remove any oxides present on the pyrite surface the sample was immersed in a 1 M HCl solution for 8 h. After rinsing the cubes in deoxygenated UHQ-water and drying them in the glovebox, they were crushed using an agate grinding mill. The powdered pyrite was cleaned once more in 1 M HCl solution for 1 h. Subsequently, the acid solution was decanted and the pyrite was rinsed with deoxygenated UHQ-water. To separate different size fractions, the pyrite suspension was wet sieved using mesh sizes of 63 μm and 30 μm, with the largest fraction used for MEO being 30–63 μm (large). The fine fraction (< 30 μm) was separated into two fractions. To this end, the pyrite suspension was shaken in a 5 mL glass tube and the fraction that was still suspended after 3 min contained the fine size fraction (mode 6 μm; < 10 μm, fine) while the fraction that had settled on the bottom of the 5 mL glass tube within 3 min contained the medium fraction (mode 22 μm; 2–63 μm, medium). The solid concentrations in the suspensions were 1.75 g/L for the fine, 45.6 g/L for the medium and 24 g/L for the coarse size fraction. Siderite originating from Queenstown, Quebec, Canada (obtained from Ward's Natural Science Establishment) was ground by agate grinding mill and suspended in deoxygenated UHQ-water (10 g/L). Following the procedure above, the finest size fraction was obtained from the supernatant during sedimentation. The solid concentration of the suspension was 10.7 g/L and the mode of the size distribution of the suspended particles was 17.8 μm.

Mixtures of chemically reduced smectite SWa-1, fine pyrite and siderite were prepared by combining the corresponding suspensions. An overview of the samples used in this study is given in Table 1.

Results from the characterization of the various minerals are presented in the Supporting Information (SI). Total element concentrations of the Boom Clay sample were obtained by total reflection X-ray fluorescence spectroscopy (TXRF, S2 Picofox, Bruker), and by digestion of the minerals in a heated mixture of HF, HNO_3 and $HClO_4$ (Reitz et al., 2004) followed by ICP-OES analysis (Spectro Arcos). The minerals were qualitatively characterized by X-ray diffraction (XRD, Co-source; D2 PHASER from Bruker with a LINXEYE™ detector). Quantitative mineral characterization by XRD was performed on a different slice of the same core at depth 75.36 m by Qmineral, Leuven, Belgium. A detailed description of this method is given in Koenen and Griffioen (2016). Organic carbon content was determined using an elemental analyzer (Fison Instruments, model NA 1500 NCS) after carbonates had been removed from the sample by repeated washing with 1 M HCl. The Boom Clay sample was subjected to a sequential Fe-extraction according to Claff et al. (2010) with some additional modifications. The extraction step targeting crystalline Fe-Oxides was altered to a repeated addition of 0.5 g of Na-dithionite per g Boom Clay with a reaction time of 10 min per addition at a temperature of 70 °C. The final step, the digestion of Fe in Al-silicates, was replaced by the HF digestion method as mentioned above. Fe concentrations in the extraction solutions were determined by ICP-OES. For extraction step 2 using 1 M HCl, the ferrozine colorimetric method (Viollier et al., 2000) was used to measure the Fe^{II} concentration. Boom Clay samples from neighboring cores KB103 and KB101, collected at similar depths but at an approximate horizontal distance of 250 m from KB104 (Behrends et al., 2016), were analyzed by Mössbauer spectroscopy. The spectra were collected at both room temperature (300 K) and at liquid helium temperature (4.2 K) to obtain more information on the oxidation state and structural coordination of Fe. Additionally, the pyrite samples and Boom Clay sample were analyzed with scanning electron microscopy (SEM). Particle size distributions of pyrite, siderite and Boom Clay samples were examined using a Mastersizer S long bed Ver. 2.18 (Malvern Instruments Ltd.).

2.2. Electrochemical analyses

2.2.1. Set-up

The electrochemical analyses were conducted with a CHI1000C potentiostat (CH Instruments, Austin, TX, USA). Each electrochemical cell had a three-electrode setup with a 3 M NaCl Ag/AgCl reference electrode, a platinum wire counter electrode separated from working electrode compartment by a porous glass frit (Bio-Logic, Claix, France), and a glassy carbon crucible working electrode (9 mL volume, GAZ1, HTW Hochtemperatur-Werkstoffe GmbH, Thierhaupten, Germany). The working electrode also functioned as the vessel containing the electrolyte into which the two other electrodes were immersed (Fig. 1). The solution in the cell contained 0.1 M $NaClO_4$ as a background electrolyte and was buffered to pH 7.5 (0.1 M MOPS). The cells were continuously stirred using a magnetic stirring bar and plate stirrer (850 rpm).

2.2.2. Mediated electrochemical oxidation and reduction

To quantify the electron donating and accepting capacities (EDC and EAC) of the Boom Clay sediment and of the reference standards of illite, smectite, pyrite and siderite, suspensions of the respective materials were pipetted into the electrochemical cell operated in MEO and MER modes, respectively (for pyrite and siderite only MEO was investigated since these minerals are reduced and are thus electrochemically inactive in MER). By applying a constant potential, the redox-active material reacted by either donating electrons to the working electrode (MEO, applied potential of $E_H = +0.61$ V vs standard hydrogen electrode, SHE), or by accepting electrons from the working electrode (MER, $E_H = -0.6$ V vs SHE). Electron transfer mediators were used to facilitate the electron transfer between the solid sample particles and the working electrode in both MEO and MER. Descriptions of suitable mediators can be found in Gorski et al. (2012b). In this work, 2,2′-azino-bis(3-ethylbenzothiazoline-6-sulphonic acid) (ABTS; standard reduction potential $E_H^0 = +0.70$ V) and 1,1′-trimethylene-2,2′-bipyridyl (triquat, $E_H^0 = -0.54$ V) were used for MEO and MER, respectively. To measure EDC and EAC, first the mediator was added to the polarized cell in a quantity that was about

Table 1
Overview and description of samples used in this study for mediated electrochemical oxidation and reduction.

Sample	Description
SWa-1	Ferruginous smectite, Grant County, Washington, USA. Natural sample: original oxidized redox state, dithionite reduced sample: SWa-1 reduced by dithionite treatment.
SWy-1	Montmorillonite, Crook County, Wyoming, USA. Natural sample and dithionite-reduced sample.
Fithian illite	Fithian gray shale illite, Illinois, USA. Natural sample and dithionite-reduced sample.
IMt-1	Cambrian shale illite, Silver Hill, Montana, USA. Natural sample and dithionite-reduced sample.
Pyrite	Cubic, hydrothermal pyrite, Zacatecas, Mexico. Separated size fractions: Fine: < ~10 μm, Medium: ~10–30 μm, Coarse: ~30–60 μm.
Siderite	Siderite, Queenstown, Quebec, Canada.
Clay-pyrite	Mixture of 70 wt% dithionite-reduced SWa-1 and 30 wt% fine pyrite.
Pyrite-clay	Mixture of 70 wt% fine pyrite and 30 wt% dithionite-reduced SWa-1.
Clay-siderite	Mixture of 70 wt% dithionite-reduced SWa-1 and 30 wt% siderite.
Siderite-clay	Mixture of 70 wt% siderite and 30 wt% dithionite-reduced SWa-1.
Siderite-pyrite	Mixture of 70 wt% siderite and 30 wt% fine pyrite
Pyrite-siderite	Mixture of 70 wt% fine pyrite and 30 wt% siderite
Boom Clay (BC)	Boom Clay sample from a core in Zeeland, The Netherlands at 57.7 m depth

10 times higher than the expected electron transfer capacity of the added sample. After redox equilibration of the mediator to the E_H applied to the working electrode, small volumes of around 20 μL of the mineral suspensions were added to the electrochemical cells. The electrons transferred to and from the samples were directly measured in the form of oxidative or reductive current responses (C/s = A). EDC and EAC were calculated by determining the peak area of the current response (oxidative current peak for EDC, reductive current peak for EAC) using the following equation.

$$\text{EDC (or EAC)} = \frac{\frac{1}{F}\int_{t1}^{t2} I(t)\,dt}{m} \quad (1)$$

where units of EDC and EAC are mol electrons (e^-)/g sample, F is the Faraday constant (96,485 s A mol^{-1}), t_1 and t_2 (s) are the start and end of the current peak, I(t) (A) is the current as a function of time and m (g) is the mass of the amount of sample added. Each sample was analyzed at least three times.

3. Results and discussion

3.1. Characterization of Boom Clay sample

Analysis of the XRD pattern of the Boom Clay sample (SI, Fig. S.1) indicates that the main mineralogy consisted of quartz, K-feldspar, Na-plagioclase, pyrite and clay minerals. The spectrum acquired did not allow differentiating different clay minerals that were present in the sample. However, quantitative XRD of a neighboring sample slice (SI, Table S.1) showed that the main clay minerals present were smectite (46 wt%), illite (16 wt%), mixed-layer illite-smectite (29 wt%), kaolinite (7 wt%), mixed-layer kaolinite-smectite (3 wt%) and chloritic minerals (1 wt%). Similar clay mineral contents were found in studies on Boom Clay samples in Belgium (e.g. Honty and De Craen, 2012; Zeelmaekers, 2011). Results from sequential Fe-extraction (Fig. 2b and SI, Fig. S.2) showed that most Fe (334 ± 2 μmol Fe/g BC) was extracted in the HF step targeting clay minerals. The second largest Fe pool (61 ± 6 μmol Fe/g BC) was extracted by treatment with concentrated HNO_3 targeting pyrite. The 1 M HCl step, potentially dissolving FeS, $FeCO_3$ and amorphous Fe(oxyhydr)oxides, extracted around 20 μmol Fe/g. The ferrozine method indicated that 16 ± 3 μmol/g BC of the HCl-extracted Fe was in the form of Fe^{2+} and 3.8 ± 0.6 μmol/g BC was Fe^{3+}. A similar amount of around 20 μmol Fe/g was extracted in the citrate-bicarbonate buffered dithionite (CDB). CDB targets crystalline Fe-oxides, although minor amounts of Fe in clay minerals may also be released in this step. To analyze the redox state of Fe in the clay minerals, Mössbauer analysis was performed on two samples of neighboring cores (Fig. 2a). The procedure of fitting the Mössbauer spectra is described in detail in the Supplementary information (SI, Table S.2). The spectral contributions of the two samples were averaged with the difference between the two as error. The largest spectral contribution came from octahedral Fe^{III} (59 ± 8%), which was distributed between an inner and an outer doublet (oct1 and oct2). At 4 K, a hyperfine magnetic sextuplet was observed, which was attributed to the presence of a very small amount of Fe-oxides (6 ± 3%) (error represents fitting error since only one sample was measured at 4 K). The second largest contribution came from octahedral Fe^{II}, for which also two doublets were visible. The spectrum at 4 K identified one of these doublets as siderite based on its characteristic spectrum having a magnetic hyperfine field of 17 T (Wade et al., 1999), resulting in 14 ± 2% Fe^{II} in clay minerals and 7 ± 3% from siderite. Pyrite contributed with 14 ± 3% to the spectrum. The fitted parameters of the components are listed in Table

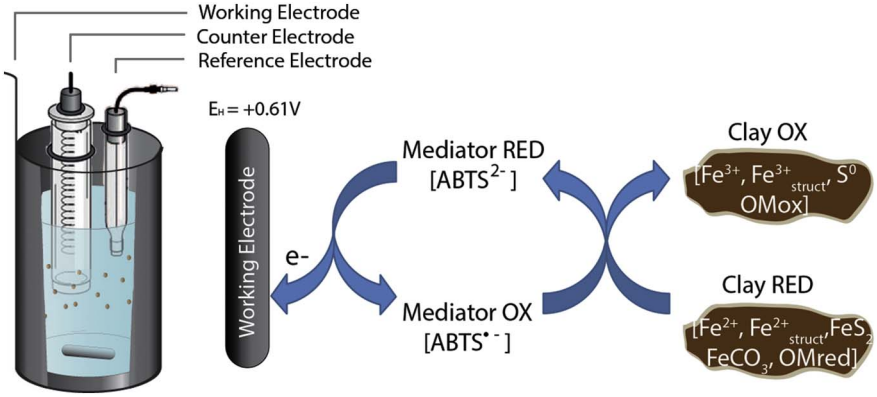

Fig. 1. Left: set-up of electrochemical cell used for mediated electrochemical analysis. Right: the reaction scheme of mediated electrochemical oxidation (MEO) of a Boom Clay sample, here with an applied potential of E_H = + 0.61 V vs standard hydrogen electrode.

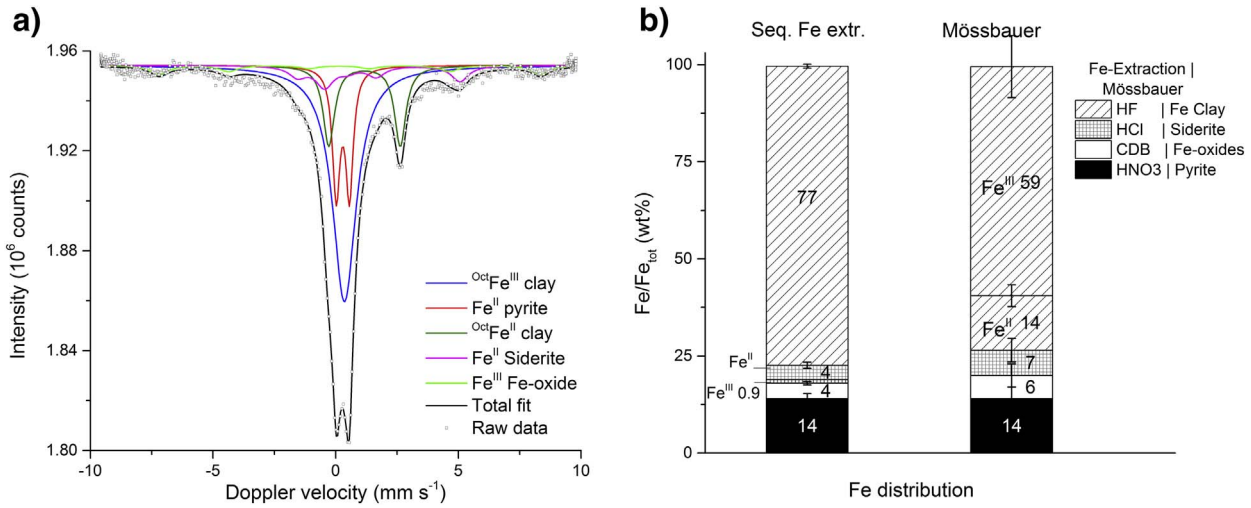

Fig. 2. a. ^{57}Fe Mössbauer spectra of a Boom Clay sample from core 103, neighboring the sample used for mediated electrochemical oxidation (MEO), collected at 4.3 K. b. Comparison of Fe distribution (wt% of total Fe) measured by sequential Fe extraction and obtained from Mössbauer analysis.

S.2. The Fe pools obtained by sequential Fe-extraction and from Mössbauer spectra give similar results (Fig. 2b). Next to Fe phases another possibly redox-active constituent is organic matter. The Boom Clay sample had an organic matter content of 0.43 wt% C. Since the in-situ sediment resides under reducing conditions and because the reductive capacity is most relevant for radionuclide retention, we focused on determining the electron donating capacity (EDC) obtained by mediated electrochemical oxidation (MEO). Organic matter and structural Fe in smectites have already been extensively investigated with both MEO and MER (e.g. Aeschbacher et al., 2011, 2010; Gorski et al., 2012a, 2012b). MEO and MER of illite have not been investigated yet. Although structural Fe^{III} is often predominant in illites, structural Fe^{II} can be present (Johnston and Cardile, 1987; Murad and Wagner, 1994). To a varying extent, structural Fe^{III} in illite can be microbially reduced (e.g. (Jaisi et al., 2007; Seabaugh et al., 2006) and structural Fe^{II} in chemically reduced illites has been shown to be redox-active towards Cr^{VI} (Taylor et al., 2000). Besides illite, the response of pyrite and siderite in MEO has also not been previously determined. To include these minerals in the interpretation of the combined oxidative current of all the constituents in the Boom Clay, we first investigated the electro-activity of the separate minerals in MEO. For this, standard minerals of illite, pyrite and siderite were used as a model for their counter parts in Boom Clay.

3.2. Mediated electrochemical oxidation and reduction of clay minerals, pyrite and siderite

3.2.1. Clay minerals

Several standard smectite clay minerals have been analyzed by MEO and MER in the Gorski et al.'s study (Gorski et al., 2012a). They observed sharp reductive and oxidative current responses of these clay materials in MEO and MER, respectively. All of the structural Fe in the reference smectites, SWa-1 and SWy-2, was found to be electro-active in MEO and MER. To validate the electrochemical cell set-up used in this work and to have a well-defined reference against which we could compare the mediated electrochemical analysis results of the other minerals analyzed here, we re-analyzed SWa-1 and SWy-2. In this study we used the original SWy-1 instead of SWy-2. SWy-2 is the second batch of Wyoming smectite reference material from the Clay Minerals Society. This second batch was collected and prepared after the first batch, SWy-1, was depleted. It was sampled from the same formation on the same location at the same site. SWy-1 and SWy-2 are generally considered to have similar properties. Current responses for the clay minerals in MEO are shown in Fig. 3a and b, and for MER in Fig. S.5 of the Supporting information. MER of the natural (oxidized) smectites and MEO of the dithionite-reduced smectites resulted in sharp current peaks. For natural SWa-1, integration of the reductive current peaks according to Eq. (1) yielded an EAC value of 2.1 ± 0.1 mmol e^-/g, which was in very good agreement with the total amount of structural Fe in this clay (i.e., 2.0 ± 0.3 mmol Fe_{struct}/g). Similarly, all structural Fe in natural SWy-1 was present as Fe^{III} and fully reducible in MER (i.e., EA-C = 0.43 ± 0.04 mmol e^-/g as compared to 0.46 ± 0.02 Fe_{struct}/g). Both dithionite-reduced smectites yielded small reductive current peaks in MER suggesting that the dithionite-reduction of structural Fe^{III} was incomplete. However, the sum of EDC and EAC values of the dithionite-reduced (2.2 ± 0.07 mmol e^-/g) did not significantly differ from the EAC of the natural, oxidized SWa-1. The same holds true for the dithionite-reduced SWy-1 (EAC + EDC: 0.38 ± 0.03 mmol e^-/g). These findings confirm the results reported by Gorski et al. (2012a) that in both natural and dithionite-reduced SWa-1 and SWy-1 all structural Fe was electro-active in MER and MEO (Fig. 4). Furthermore, the good agreement validates the accuracy of the MEO and MER setup used in this work.

For the two illites, Fithian illite and IMt-1, the oxidative and reductive current peaks in MEO and MER were also very sharp (shown for MEO of chemically-reduced clays in Fig. 3b). Integration of the reductive current peaks obtained for the natural illites in MER resulted in an EAC value of 0.16 ± 0.01 mmol e^-/g for the Fithian Illite, corresponding to 21.9 ± 2.1% of the total structural Fe (Fe_{struct}) and 0.09 ± 0.01 mmol e^-/g for IMt-1, corresponding to 11.4 ± 1.7% of total Fe_{struct} (Fig. 4). Only a comparatively small fraction of the Fe_{struct} in illites appeared to be reducible in MER. The dithionite-reduction treatment, like for the smectites, reduced most but not all electro-active Fe_{struct} present in the natural illites, as evidenced from small reductive current responses in MER and larger oxidative current responses in MEO of the reduced illites. The sum of EDC and EAC of dithionite-reduced Fithian illite was 0.19 ± 0.01 mmol e^-/g, which is slightly higher than the EAC of the natural, oxidized sample. It is possible that the dithionite treatment activated a small amount of the Fe_{struct} that was unavailable to electron transfer with the mediator in the native Fithian illite. The sum of EDC and EAC of dithionite-reduced IMt-1 was 0.11 ± 0.01 mmol e^-/g which corresponds well to the EAC of the natural, oxidized IMt-1. This finding implies that the chemical reduction step did not significantly alter the pool of electrochemically active Fe and that all electrochemically active Fe in the oxidized illite samples was present as Fe^{III}.

The electro-activity of Fe in illites determined by mediated electrochemical analysis can be compared to a study on microbial reduction of

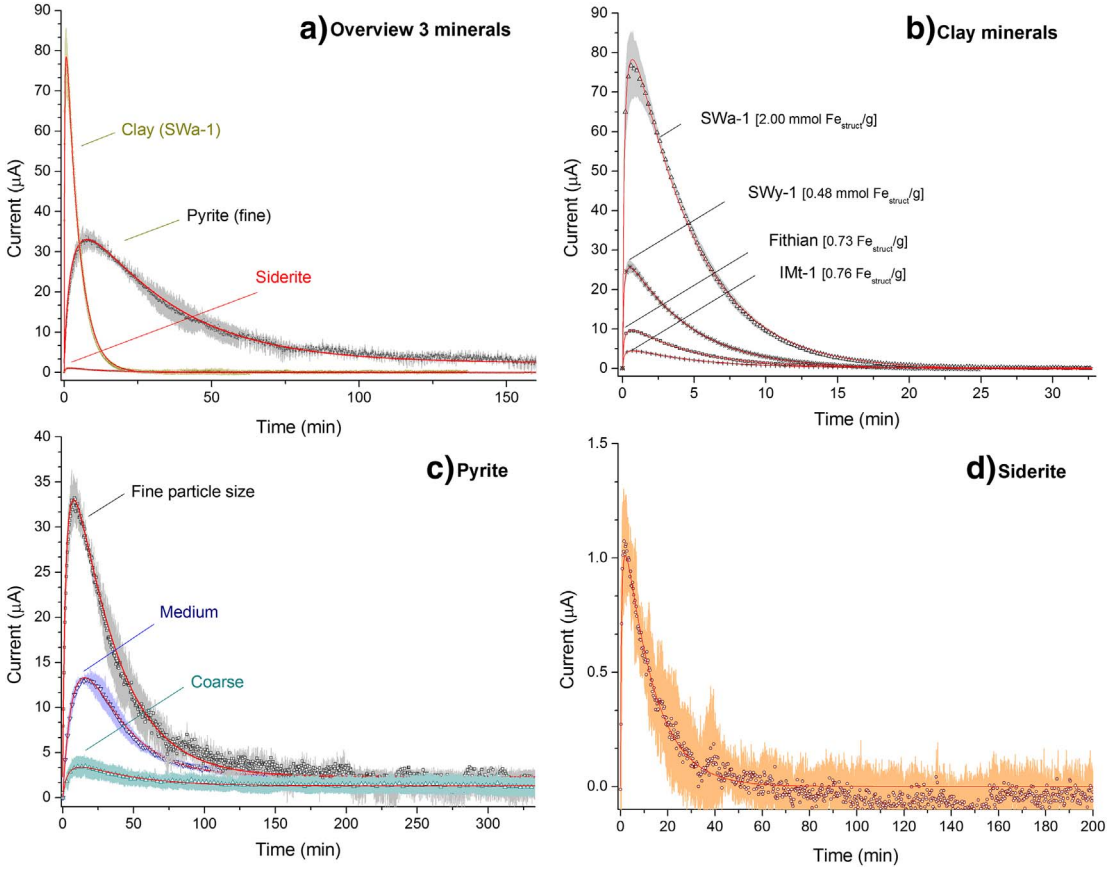

Fig. 3. Baseline corrected oxidative current responses in mediated electrochemical oxidation (MEO) to additions of 0.2 mg of different minerals: a. dithionite-reduced clay mineral SWa-1, siderite and fine pyrite, b. siderite, c. fine, medium and large coarse pyrite, d. dithionite-reduced SWa-1, SWy-1, Fithian illite and IMt-1. Shades around data points represent the range of duplicate measurements (fine pyrite), or the standard deviation of triplicate measurements (clay minerals), or six replications (all other). Red lines through data points are curves fitted with the empirical Eq. (4). For clarity not all data points are presented by a symbol, e.g. for coarse pyrite every fortieth and for clay minerals every fifth data point is displayed. (For interpretation of the references to color in this figure legend, the reader is referred to the web version of this article.)

illites in the presence of an electron shuttle, anthraquinone-2,6-disulfonate (AQDS) (Seabaugh et al., 2006). They report that 20 to 25% of Fithian illite-associated Fe^{III} can be reduced microbially, which is in good agreement with our finding that only a comparatively small fraction of total Fe was electro-active in mediated electrochemistry. This suggests that structural Fe^{III} in illite accessible to mediated electrochemical analyses is also redox-active in microbial reduction experiments. This may indicate that the electro-active fraction of structural Fe determined by MER and MEO could be used to constrain the fraction of Fe in illites that is redox-active in natural biogeochemical processes. For smectites, the extent of microbial reduction of structural Fe in SWa-1 has been shown to be 46% to > 90% depending on the bacterial community (Kostka et al., 1999). For nontronite NAu-2, Luan et al. (2014) showed that the extent of Fe_{struct} reduction is dependent on reduction potential, which was also shown for SWa-1 by Gorski et al. (Gorski et al., 2012b). This needs to be taken into account when using the fraction of electro-active Fe_{struct}, measured by mediated electrochemistry, for predictions of redox-activity in natural biogeochemical processes. The electro-active fraction of structural Fe in IMt-1 was lower than in the Fithian illite. Previous work has suggested that fractions of electro-active Fe may decrease with increasing structural Fe contents, possibly due to the inability of the clay minerals to make structural re-arrangements required for charge balancing (Gorski et al., 2012a; Seabaugh et al., 2006). However, this explanation does not apply to the two illites analyzed here because of their similar Fe contents (Fithian: 4.4%, IMt-1: 4.6%). Alternatively, the difference in electro-active Fe between the illites may originate from differences in layer charge (Fithian illite: ~0.56 eq/half unit cell (Seabaugh et al., 2006), IMt-1: ~0.72 eq/half unit cell (Malla et al., 1993)), mineral surface area, and from differences in arrangement of Fe in the octahedral sheet (Gaudette, 1964; Liu et al., 2012; Neumann et al., 2011b; Seabaugh et al., 2006). Differences in these mineral properties probably also explain the contrast between electro-activity of structural Fe in smectite and illite. The larger layer charge of illites results in lower interlayer expandabilities compared to smectites and consequently lower accessibility of structural Fe-sites to electron shuttles (Liu et al., 2012; Seabaugh et al., 2006). Finally, differences in the coordination and arrangement of structural Fe in smectites and illites may further affect the availability of structural Fe for reduction and oxidation (Gorski et al., 2013; Neumann et al., 2011a, 2011b).

3.2.2. *Pyrite and siderite*

Electron transfer in mediated electrochemical oxidation of pyrite was significantly slower compared to the clay minerals (Fig. 3a). The maximum oxidative currents were reached between approximately 340 and 1140 s after pyrite addition, while maximum oxidative currents were reached in less than 40 s after clay mineral additions. Fig. 3c displays the oxidative current responses to additions of 0.2 mg pyrite of the three different size fractions. Pyrite oxidation kinetics became slower with increasing nominal particle size: the time periods, after pyrite addition, required to attain maximum oxidative current values and to re-approach background current values following the current peak, increased with increasing pyrite grain size. In general, the oxidative currents did not re-attain background current values of 1 µA over the time frame of the measurements but instead remained elevated between 2 and 5 µA. Consistent with the decelerating oxidation kinetics with increasing particle size, the EDC values decreased with increasing particle size: from 14 ± 2 mmol e^-/g for the finest size fraction, to

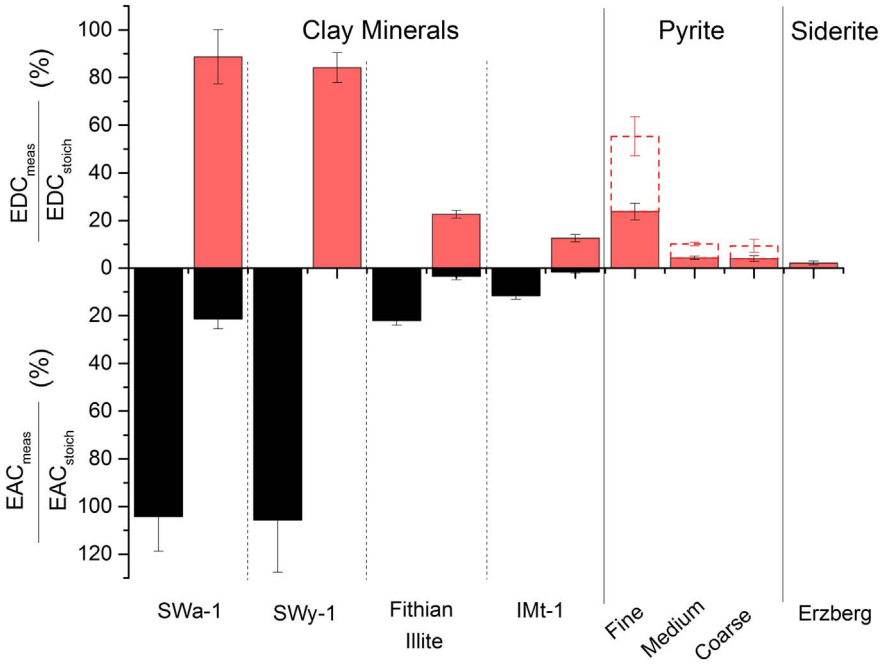

Fig. 4. Ratios of the measured electron donating capacities (EDC, red bars) and electron accepting capacities (EAC, black bars) over the theoretical, calculated EDC and EAC values of four standard reference clays (natural or dithionite-reduced), of different size fractions of pyrite and of siderite. The expected EDC and EAC values for clay minerals were calculated based on the structural Fe content of the clay minerals and a stoichiometry of 1 mol transferred e^- per oxidation or reduction of 1 mol structural Fe. For siderite also a stoichiometry of 1 mol released e^- per 1 mol oxidized Fe^{II} was used. For pyrite two oxidation reactions were considered: 1 mol of pyrite releases 3 mol e^- (dashed line)(oxidation to S^0 and Fe^{III}) or 7 mol e^- (solid line)(oxidation to $S_2O_3^{2-}$). Error bars represent propagated error of measured structural Fe (duplicates) and standard deviations of repeated electrochemical measurements with $n = 3$ for clay minerals and fine and medium sized pyrite, $n = 5$ for coarse pyrite and $n = 9$ for siderite. (For interpretation of the references to color in this figure legend, the reader is referred to the web version of this article.)

2.7 ± 0.18 mmol e^-/g and 2.3 ± 0.7 mmol e^-/g for the medium and coarse fraction of pyrite, respectively (Fig. 4). The pyrite tested here was cubic, whereas pyrite in natural clays such as Boom Clay is predominantly present in framboidal form. We therefore also measured MEO of synthesized framboidal pyrite (SI, Fig. S.8d) which did not show any major differences compared to that of the fine (cubic) pyrite (SI, Fig. S.9). The trend of decreasing EDC with increasing particle size indicates that the extent of pyrite oxidation is size dependent and, when assuming the reaction stoichiometry is the same for all size fractions of pyrite, suggests that oxidation is incomplete. In order to evaluate the yield of pyrite oxidation based on EDC, the stoichiometry of the oxidation reaction needs to be known.

It is unclear which primary oxidation products form during mediated electrochemical oxidation of pyrite under anoxic conditions. With elemental oxygen or dissolved Fe^{3+} as oxidants for pyrite in aqueous solution, intermediate formation of sulfoxy anions has been reported and eventually sulfate is considered the main sulfur product of pyrite oxidation (Goldhaber, 1983; Moses et al., 1987; Moses and Herman, 1991). However, for anaerobic electrochemical oxidation of pyrite at applied potentials ≤ 0.6 V vs SHE, XPS and Raman spectroscopy measurements have shown that S^0 can be a product (Holmes and Crundwell, 2000; Kelsall et al., 1999; Mycroft et al., 1990; Turcotte et al., 1993; Hamilton and Woods, 1981). At potentials below 0.6 V, $S_2O_3^{2-}$ and S^0 are expected to form, while further oxidation to SO_4^{2-} is expected to be of minor importance (Kelsall et al., 1999). Elemental sulfur, as a product of pyrite oxidation, is thought to form by the decomposition of the intermediate oxidation product $S_2O_3^{2-}$ that is unstable under acidic conditions (Kelsall et al., 1999; Moses et al., 1987). Under alkaline conditions, $S_2O_3^{2-}$ is more stable and does not decompose quickly to S^0 (Kelsall et al., 1999; Xu and Schoonen, 1995). The products expected for electrochemical oxidation of pyrite under alkaline to circumneutral pH and at a reduction potential around E_H = 0.6 V vs SHE include $Fe(OH)_3$, $S_2O_3^{2-}$ and S^0 and possibly traces of SO_4^{2-} as well as intermediate polysulfides.

The oxidation of pyrite to S^0 and $Fe(OH)_3$ as major oxidation products would result in donation of 3 mol e^- per mole pyrite and therefore a theoretical EDC value of 25 mmol e^-/g. Oxidation to $S_2O_3^{2-}$ and $Fe(OH)_3$ would result in a 7 mol e^- transfer per mole pyrite which corresponds to a theoretical EDC value of 58.3 mmol e^-/g. Both theoretical EDC values are much larger than the measured EDC values for pyrite, which were between 14 and 2.3 mmol e^-/g depending on the size fraction tested. Incomplete oxidation of pyrite over the course of MEO and the strong dependency of oxidation rates and extents on particle size can be attributed to surface processes such as the loss of reactive surface sites and the formation of oxidation products on the pyrite particle surface. Under acidic conditions, lower oxidation rates were observed in biological experiments when sulfur accumulation at the pyrite surface was detected (Sasaki et al., 1998). Surface passivation, most likely by accumulated sulfur, was also observed by Long and Dixon (2004). At pH 7.5, applied in our experiments, $S_2O_3^{2-}$ is more stable and S^0 less likely to form. Here, slow oxidation could also arise from the fact that at potentials below 0.6 V several steps in the oxidation process are very slow and oxidation is likely to occur exclusively at defects, steps and kinks at the pyrite surface (Kelsall et al., 1999a). The loss of these reactive surface sites will slow down the oxidation process of the pyrite even more which may result in very low currents. Furthermore, formation of a surface layer of ferric iron (oxyhydr)oxides (Caldeira et al., 2003; Todd and Sherman, 2003) at alkaline pH could also possibly slow down the oxidation of pyrite. Poisoning of the electrode may have caused loss of reactivity. However, the potential amounts of formed S^0 would have been very small in comparison to the working electrode surface. It is also more likely that S^0 formed on the mineral surface rather than the electrode surface due to the fact that the electron transfer in MEO was mediated.

The addition of siderite to MEO cells resulted in only a very small oxidative current peak (Fig. 3a and d). Integration of the oxidative current peaks showed that less than 2.1 ± 0.8% of the Fe^{II} in siderite was oxidized over the course of MEO. Under the MEO conditions used

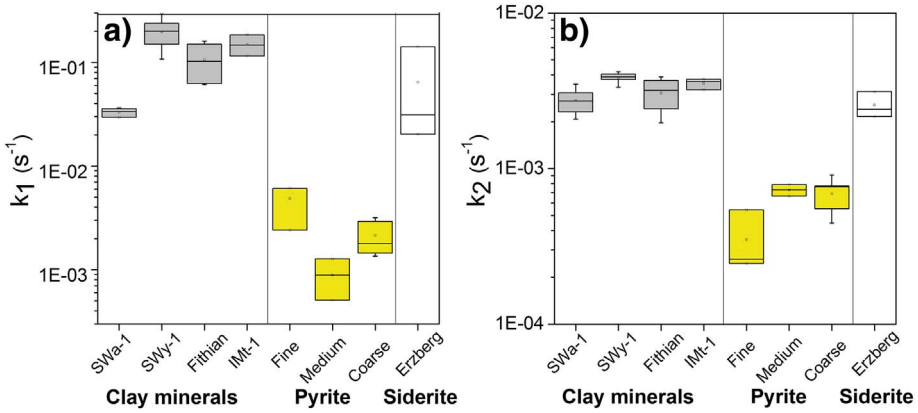

Fig. 5. Box plots of parameters k_1 (a) and k_2 (b) from Eq. (4) for various clay minerals, pyrite of different grain sizes and siderite. The parameter values were obtained by fitting Eq. (4) to the oxidative current peaks measured in mediated electrochemical oxidation in response to mineral additions.

here, structurally bound Fe^{II} in carbonates was therefore not electroactive. Photochemical (Kim et al., 2013) and chemical (Duckworth and Martin, 2004; Rakshit et al., 2008) oxidation of siderite is coupled to the formation of iron oxides, implying that the reaction proceeds via a dissolution-precipitation mechanism. Hence, the measured currents could be explained by oxidation of surface-bound Fe^{II} and/or aqueous Fe^{II} released into solution during slow siderite dissolution. Siderite has a structure similar to calcite. Assuming a surface density of 1 Fe atom/20 $Å^2$ (Stipp, 1999; Turner et al., 2014; Walter and Morse, 1984), a surface roughness of 1 and a particle size of 17.8 μm, a concentration of 1.8 μmol surface Fe/g siderite is obtained. This represents about 0.01% of bulk Fe content of siderite. The latter implies that oxidation of surface-bound Fe^{II} alone cannot explain the measured EDC. It is therefore conceivable that aqueous Fe^{II} released by siderite dissolution could account for the observed currents. Dissolved Fe^{II} readily undergoes electrochemical oxidation with or without mediators. At conditions comparable to those in the MEO measurements, Duckworth and Martin (2004) found a dissolution rate of $10^{-8.5}$ mol m^{-2} s^{-1} which corresponds at steady state conditions to a current of about 7.6 nA for the 2 mg siderite used in the MEO experiment. This is lower than the measured background current and can therefore not explain the small observed current peak. Grinding and size separation of the siderite sample, could have formed labile Fe on the siderite surface which can possibly explain the small current peak.

3.3. Fitting of current peaks

The pronounced difference in oxidation kinetics of clay minerals and pyrite in MEO offers the opportunity to separate their contributions to the overall oxidative current responses obtained in MEO when analyzing samples that contain a mixture of these minerals. For this purpose, we developed an empirical equation describing the current responses in MEO for the analyzed pyrite, siderite and clay minerals. A first-order rate law can be used to describe the decrease in the oxidative currents after the maximum peak current.

$$I(t) = I_0 \bullet e^{-k \bullet t} \quad (2)$$

where I(t) (A) is the current at a given time t(s), I_0 (A) is a virtual initial current at time zero. The decay constant, k (s^{-1}), is a measure of the steepness of the current decrease.

The measured oxidative currents depend on the rates at which electrons are transferred to the working electrode. This rate may be limited by different steps in the mediated oxidation process (Fig. 1). The decay constant k describes the overall rate determining step in MEO. Information on the electron transfer rates from the mineral sample to the mediator (and the corresponding k-value) can only be obtained if this transfer step is slower than the rate at which the mediator is re-oxidized at the working electrode (i.e. the combined rate for mass transfer of the reduced mediator to the working electrode and for the re-oxidation of the reduced mediator at the working electrode). The kinetics of electrochemical mediator oxidation were obtained by fitting Eq. (2) to the oxidative current peak generated by addition of ABTS-mediator to the electrochemical cell prior to the addition of the mineral samples. The k-value for oxidation of ABTS-mediator of 0.0047 s^{-1} was much larger than the k-values obtained by fitting the current responses of the mineral samples (k_2 in Fig. 5). The current responses to mineral additions measured in MEO therefore reflected the rates at which electrons were transferred from the added minerals to the $ABTS^{\bullet+}$ and not the rates of ABTS re-oxidation.

While Eq. (2) describes the decline of the oxidative current peak, it cannot describe the onset of the initial part of the oxidative current peak during which the current (slowly) increased up to a maximum peak value. Ideally, an immediate increase to maximum current values is expected followed by a decrease in current as the material is consumed by oxidation. An initial increase in current however, suggests that oxidation accelerates over time. The process(es) underlying this initial increase remain(s) unclear, although it appeared that these initial current increases were mineral specific. That is, the initial increases were fast for clay minerals and siderite but slow for pyrite. We also observed that aging of suspensions of fine pyrite resulted in slower initial current increases (SI, Fig. S.10b). This aging effect may have originated from observed particle aggregation which decreases the mediator-accessible surface of the mineral at the beginning of the measurements. Through time, possibly by rigorous stirring, the particles disperse and consequently more sites become available. While the causation behind the initial increase in the oxidative currents remains unclear, we found that the initial current increase can be described by an asymptotic function:

$$I(t) = \frac{k_I \bullet t}{k_I \bullet t + 1} \quad (3)$$

To describe the total oxidative current peaks Eqs. (2) and (3) were combined:

$$I(t) = A \bullet \frac{k_I \bullet t}{k_I \bullet t + 1} \bullet e^{-k_2 \bullet t} + B \quad (4)$$

where B (A) accounts for the background current and A (A) is a scaling factor to adjust the peak height to the measured maximum current. With this generic function it was possible to accurately fit the oxidative current peaks of all analyzed reference materials (Fig. 3a–d). The fitting procedure was performed by least squares regression with an iteration procedure based on Levenberg-Marquardt algorithm. The fitted values for k_1 and k_2 were significantly smaller for pyrite than for all clay minerals (Fig. 5). The values for k_1 were in the range of $1.2–6.1 \cdot 10^{-3}$ s^{-1} for pyrite, $20–140 \cdot 10^{-3}$ s^{-1} for siderite and $27–240 \cdot 10^{-3}$ s^{-1} for clay minerals. k_1-values varied considerably

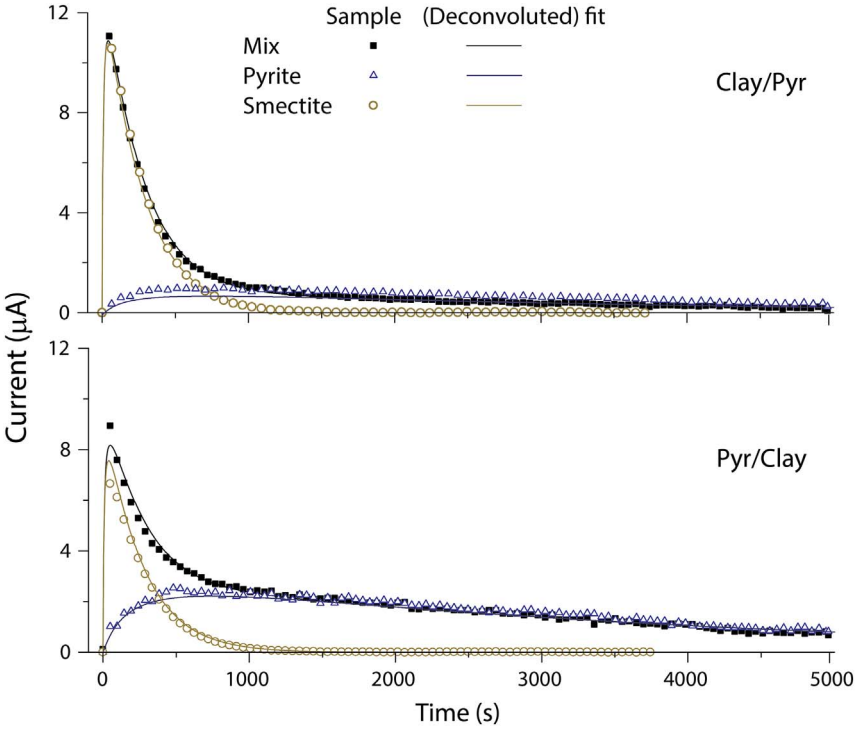

Fig. 6. Baseline corrected oxidative current responses in mediated electrochemical oxidation (MEO) of mineral mixtures clay-pyrite (70 wt%–30 wt%) and pyrite-clay (30 wt%–70 wt%) (filled black squares). The black line represents the fitted curve using Eq. (5) with constrained k-values, and the beige and blue lines are the deconvoluted curves for clay and pyrite in the mixture, respectively. The open symbols are measured current responses to MEO of individually measured SWa-1 (open circles) and fine pyrite (open triangles). (For interpretation of the references to color in this figure legend, the reader is referred to the web version of this article.)

between different clay minerals and between pyrites of different particle size. In contrast, values for k_2 were all similar for the various clay minerals with an average of $3.2 \pm 0.7 \cdot 10^{-3}\,s^{-1}$. For pyrite, the average k_2 value was $0.59 \pm 0.23 \cdot 10^{-3}\,s^{-1}$ and for siderite $2.6 \pm 0.5 \cdot 10^{-3}\,s^{-1}$.

3.4. Mixtures of standard minerals

Before analyzing natural Boom Clay samples, we first validated that current peaks of (synthetic) mixtures of reference minerals behaved additively in terms of the current contributions of the individual minerals in the mixture. To this end, the measured current peak responses to addition of the mixtures were fitted using a linear combination of empirical Eq. (4) of the different reference materials in the mixture:

$$I_{Mix\ clay-pyr}(t) = A_{clay} \bullet \frac{k_{1clay} \bullet t}{k_{1clay} \bullet t + 1} \bullet e^{-k_{2clay} \bullet t} + A_{pyrite} \bullet \frac{k_{1pyrite} \bullet t}{k_{1pyrite} \bullet t + 1} \bullet e^{-k_{2pyrite} \bullet t} + B \quad (5)$$

In the fitting procedure (iterative least squares method) k_1- and k_2-values were constrained by the minimum and maximum values of all the previously measured individual reference minerals, i.e. k_{1clay} and k_{2clay} were constrained between the minimum and maximum values of all different clay minerals, and k_{1pyr} and k_{2pyr} by the minimum and maximum values of all pyrite particle sizes (Fig. 5). The k-values were not a-priori set to the exact values obtained from measurements of the individual materials used in the mixture in order to test the robustness of the fitting procedure. That is, to assess the suitability of the method to be applied to a sample like Boom Clay, of which the exact pyrite size and clay mineralogy are unknown. Only variables A_{clay}, A_{pyrite} and B, representing the relative quantities of the minerals in the mixture and

Table 2
Optimized parameters k_1 and k_2, obtained by fitting current peaks of the individually measured smectite clay mineral SWa-1 and fine pyrite using Eq. (4), and of mineral mixtures and Boom Clay using Eq. (5). The lower and upper limits, used for fitting the k-values in Eq. (5), are also shown.

	Clay component		Pyrite component	
	k_1 ($10^{-3}\,s^{-1}$)	k_2 ($10^{-3}\,s^{-1}$)	k_1 ($10^{-3}\,s^{-1}$)	k_2 ($10^{-3}\,s^{-1}$)
Individual minerals				
SWa-1	125 ± 42	3.97 ± 0.30	–	–
Fine pyrite	–	–	6.08 ± 0.35	0.35 ± 0.17
Lower and upper boundaries of k-values in Eq. (5)				
	27–240	1.97–4.19	1.2–6.1	0.24–0.77
Mixtures and natural sediment				
Clay-Pyr	152 ± 53	4.19 ± 0	4.17 ± 2.73	0.38 ± 0.19
Pyr-Clay	240 ± 0	4.15 ± 0.06	1.90 ± 0.04	0.43 ± 0.03
Boom Clay	99 ± 44	3.84 ± 0.32	4.5 ± 2.8	0.56 ± 0.04

Reported uncertainties indicate standard deviations of triplicate measurements (fine pyrite) or four replicate measurements (SWa-1).

the background current, respectively, were fitted without constraints. With the optimized parameters, the overall measured current peaks were deconvoluted and the contributions of the two individual types of minerals in the mixtures were derived.

Fig. 6 shows experimentally measured and fitted current responses for the mixtures of pyrite and clay. Results for mixtures containing siderite can be found in the Supporting Information (SI, Fig. S.11). Eq. (5) reproduced the current peaks well, although the onset of the current peak for the pyrite-clay-mixture was slightly steeper than the fit could reproduce within the given k_1 boundaries (Fig. 6). Optimized k-values obtained by fitting the current peaks of the mixtures were, in general, very similar to those obtained from fitting the current curves of individually measured SWa-1 and fine pyrite that were used for the mixture (Table 2). An exception was the value of k_{1clay} for the pyrite-clay-mixture which was larger than the k_1-value of individually measured SWa-1 because the onset of the current peak of the mixture was faster than that of the individually measured SWa-1. The EDC values obtained by integrating the deconvoluted current responses were very similar to the EDC values determined for the individual minerals: the EDC values for clay and pyrite were 1.3 ± 0.1 mmol $e^-/g_{clay\ in\ mix}$ and 5.7 ± 0.2 mmol $e^-/g_{pyr\ in\ mix}$) in the mixture and 1.3 mmol e^-/g_{clay} and 5.2 ± 0.9 mmol e^-/g_{pyrite} when SWa-1 and pyrite were individually analyzed, respectively. This demonstrates that the current response for mixtures of reference materials was additive with respect to currents obtained from individual mineral components. Note that the fine pyrite used to prepare the mixtures had a slightly different grain size distribution (with more larger particles) compared to the fine pyrite analyzed in Section 3.2.2. This difference in grain size explains the lower EDC value for fine pyrite used in the mixture.

MEO of mixtures containing siderite and pyrite (pyrite-siderite 70–30% and siderite-pyrite 70–30%) resulted in current peaks similar to those obtained by MEO of individually added pyrite (SI, Fig. S.11). In the mixtures of siderite with pyrite but also in siderite with smectite, the current responses from MEO of siderite appeared to be too small to be separated from the larger current peaks produced by MEO of the other minerals.

3.5. Application of deconvolution method to MEO of a Boom Clay sample

The oxidative current response in MEO to addition of 2 mg of the Boom Clay (BC) sample showed a narrow peak with a shoulder at around 1500 s (Fig. 7). The EDC value was 0.2 ± 0.05 mmol e^-/g dry BC. Several redox-active constituents present in BC could contribute to this oxidative current peak including clay minerals, pyrite and siderite, as well as natural organic matter. MEO of natural organic matter (NOM) (i.e. humic and fulvic substances in particular) was shown to exhibit fast electron transfer kinetics with sharp current peak responses (e.g. Aeschbacher et al., 2012). Consequently, the current contribution of natural organic matter to the oxidative currents of BC samples might be difficult to distinguish from that of clay minerals. While NOM extracted from BC was not available for analysis, we had access to dissolved organic matter (DOM) from BC pore water obtained from two piezometers. The MEO of the DOM is shown in Fig. S.12 (SI). Fitting of the oxidative current peak of the pore water using Eq. (4) indeed yielded k_1 (0.17 s^{-1}) and k_2 (0.0014 s^{-1}) values close to or in the range of those of the clay minerals. Integration of the current peaks gave an EDC value of 0.48 ± 0.07 mmol e^-/L for water from the EG/BS piezometer and 0.57 ± 0.07 mmol e^-/L for water from the SPRING piezometer. The Fe^{2+} content in these samples was 0.0036 mmol/L for SPRING pore water and 0.016 mmol/L for EG/BS pore water, implying that the current response was predominately caused by DOM oxidation. When correcting for the contribution of Fe^{2+} to the EDC and normalizing to the dissolved organic carbon concentrations in the BC pore water samples, EDC values of DOM of about 2.4 mmol e^-/gC were obtained which is in the range of values measured by Walpen et al. (2016). When extrapolating the results for DOM to the total content of organic carbon in Boom Clay (0.43 wt%C) an EDC value of NOM in BC of approximately 0.01 mmol e^-/g BC is obtained, which is 5% of the total EDC of Boom Clay. In conclusion, deconvoluting the contributions of clay minerals and NOM to the oxidative current response solely based on electron transfer kinetics seems to be impossible. However, when combining the known NOM content with an educated estimation of the EDC of NOM it is possible to separate the contributions of NOM and clay minerals from the fast oxidative current response in MEO

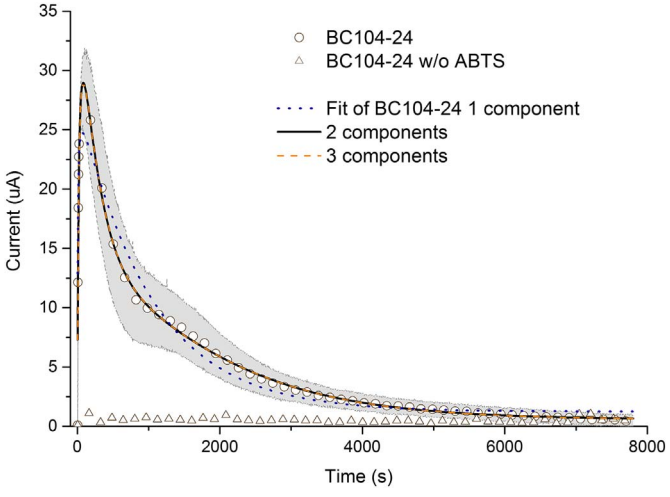

Fig. 7. Oxidative current response to the addition of 2 mg Boom Clay sample to electrochemical cells with and without ABTS as electron transfer mediator. The cell potential of the working electrode was set at E_H = 0.61 V vs SHE. Gray shade represents the standard deviation of three replicates.

The MEO current peak response to BC was fitted allowing for either one (Eq. (4)), two (Eq. (5)) and three components (Fig. 7). In the latter case, Eq. (5) was expanded by a third term for the contribution of siderite and the k-values were constrained to those obtained for siderite in the fitting procedure. As can be seen in Fig. 7 and from residual curves in Fig. S.13, using only one component was insufficient to reproduce the measured current curve. Using the model containing two components yielded a much better fit of the experimental data. Adding siderite as a third component did not improve the fit and resulted in an optimized value for A_{sid} of zero. This is in agreement with the measurements of siderite in mixtures with other reference materials: even with relatively high siderite contents, the contribution of siderite to the current response was much smaller than those from clay minerals and pyrite (SI, Fig. S.7). Consequently, from all potentially redox active constituents in BC, clay minerals and pyrite dominated the measured oxidative currents while the contribution of siderite can be neglected in a first approximation.

Integration of the deconvoluted curves obtained from the 2-component fit using Eq. (5) yielded an EDC value of 131 ± 36 µmol e^-/g BC for the pyrite fraction. The pyrite content of this sample was 61 ± 6 µmol/g BC. Recalculating the EDC value per gram pyrite yielded 17.9 ± 5.2 mmol e^-/g_{pyrite}. This value is similar to the EDC values of 14 ± 2 mmol e^-/g_{pyrite} determined for the fine-grained reference pyrite. SEM images of the sample (SI, Fig. S.4) showed that pyrite was present in varying particle sizes, but that fine particles dominated. For the fast reacting clay-NOM part of the current peak, an EDC of 42 ± 14 µmol e^-/g BC was obtained. Correcting for the estimated EDC value of NOM gave an EDC value of 32 ± 14 µmol e^-/g BC that likely originated from structural Fe^{II} in clays. Based on Mössbauer analyses of a set of surrounding Boom Clay samples, about 14 ± 2% of total Fe was present in the form of structural Fe^{II}in clay minerals. Applying this percentage to the BC sample used for MEO gives an Fe^{II} content of about 60 ± 9 µmol $Fe^{II}{}_{clay}/g$ BC. This value is about twice as high as the redox active Fe^{II} content derived from MEO, suggesting that about half of the structurally bound Fe^{II} is redox active.

The remaining structural Fe in clay, 274 μmol Fe/g BC, was in the form of Fe^{III}. Performing MER on the Boom Clay sample resulted in a narrow reductive current peak with an EAC value of 52 μmol e^-/g BC (SI, Fig. S.14). This EAC value can for a large part be assigned to a small amount of Fe-oxides (30 μmol Fe/g BC) present in the sample. We therefore conclude that the vast majority of structural Fe^{III} in this naturally reduced clay sample appears to be electrochemically inactive.

The current responses of Boom Clay, obtained in MEO, showed that pyrite was the largest electro-active pool but NOM and structural Fe^{II} in clay minerals were also (partly) electro-active under the experimental conditions. The measured electro-activity of Boom Clay is, however, not necessarily equivalent to its redox activity under natural conditions. The EDC measured by MEO may under- or overestimate the capacity of Boom Clay to reduce compounds entering the clay formation. This is due to the fact that the electrochemically measured EDC only accounted for the oxidation of Boom Clay components which reacted sufficiently fast to result in an oxidative current significantly higher than the background current in the MEO cell. Conversely, much slower redox reactions may occur in the Boom Clay over the course of days, years to millions of years, which would be too slow to be detectable in MEO. In this case, the electrochemically obtained EDC underestimated the capacity of Boom Clay to reduce e.g. oxygen or SeO_3^{2-} because the EDC value did not account for siderite oxidation and only partially accounted for pyrite oxidation. For clay minerals and NOM the extent of electron transfer can depend on reduction potential (E_H) (e.g. Aeschbacher et al., 2012; Gorski et al., 2012a; Luan et al., 2014). The E_H value of + 0.6 V and − 0.6 V vs SHE used in MEO and MER are upper and lower limits of naturally occurring reduction potentials. The EDC and EAC obtained at these potentials therefore were maximum capacities and could thereby overestimate the capacities of clay minerals and NOM to accept or donate electrons in reactions with intermediate redox potentials. To obtain EDC and EAC values for a specific redox reaction, MEO and MER should be performed at the E_H value belonging to that reaction. In the case of microbial reduction, accessibility of surface sites can also limit structural Fe^{III} reduction, especially in illites (Seabaugh et al., 2006). MER could therefore have overestimated the extent of natural redox capacities accessible for anaerobic microbial respiration.

4. Conclusions

This study demonstrates that mediated electrochemical analysis allows quantification of the electron transfer capacity of a reduced natural clay sediment. The EDC values provide a measure of the reducing capacity of a sediment. This is an integral value and, as shown, may have contributions from different mineral constituents. MEO is able to probe redox-active structural Fe in different types of clay minerals and can quantify the electro-activity of DOM. Oxidation of pyrite and siderite in MEO, under the applied conditions, is incomplete. Total EDC values of the sediment could be used to assess electron donation to contaminants in natural and engineered systems, including radionuclides in RW-repositories. However, since some minerals, like pyrite, do not undergo complete oxidation and have different oxidation products in MEO compared to other oxidative conditions or microbial oxidation, the EDC obtained by MEO could underestimate the reducing capacity. In such cases the individual contributions of the redox-active minerals in the sediments need to be examined. MEO can provide information on the rates of electron transfer and, for minerals that have very different oxidation kinetics, can be used to assess their individual contributions. This worked well for separating contributions of pyrite from clay mineral Fe_{struct}-NOM in a natural clay sediment. This information of individual contributions may also be critical for detailed geochemical modeling of pollutants in subsurface environments containing different mineral reductants that transfer electrons to contaminants at different rates.

Supporting information available

Characterization of the Boom Clay sample and reference materials (grain size, digestion, sequential Fe extraction, XRD, Mössbauer spectra, SEM images). MER of reference clay minerals and the Boom Clay sample. Results of additional MEO analyses of the siderite mixtures with both pyrite and SWa-1 and MEO current curves of fresh versus aged fine pyrite suspensions, framboidal pyrite versus cubic fine pyrite, and of Boom Clay pore water from piezometers.

Acknowledgement

We thank Iulian Dugulan (TU Delft, the Netherlands) for the Mössbauer spectroscopy measurements and interpretation. The research leading to these results has received funding from the Dutch research programme on geological disposal OPERA. OPERA is financed by the Dutch Ministry of Economic Affairs and the public limited liability company Elektriciteits-Produktiemaatschappij Zuid-Nederland (EPZ) and coordinated by The Central Organization for Radioactive Waste (COVRA).

Appendix A. Supplementary data

Supplementary data to this article can be found online at http://dx.doi.org/10.1016/j.chemgeo.2017.03.022.

References

Aertsens, M., Wemaere, I., Wouters, L., 2004. Spatial variability of transport parameters in the Boom Clay. Appl. Clay Sci. 26, 37–45. http://dx.doi.org/10.1016/j.clay.2003.09.015.

Aeschbacher, M., Graf, C., Schwarzenbach, R.P., Sander, M., 2012. Antioxidant properties of humic substances. Environ. Sci. Technol. 46, 4916–4925. http://dx.doi.org/10.1021/es300039h.

Aeschbacher, M., Sander, M., Schwarzenbach, R.P., 2010. Novel electrochemical approach to assess the redox properties of humic substances. Environ. Sci. Technol. 44, 87–93. http://dx.doi.org/10.1021/es902627p.

Aeschbacher, M., Vergari, D., Schwarzenbach, R.P., Sander, M., 2011. Electrochemical analysis of proton and electron transfer equilibria of the reducible moieties in humic acids. Environ. Sci. Technol. 45, 8385–8394. http://dx.doi.org/10.1021/es201981g.

Anderson, B.J., Jenne, E.A., 1970. Anderson_Jenne_1970_Free Fe content in ref clays.pdf. Soil Sci. 109, 163–169.

Appelo, C.A.J., Postma, D., 2005. Geochemistry, Groundwater and Pollution, second ed. A.A. Balkema, Rotterdam, the Netherlands.

Badaut, V., Schlegel, M.L., Descostes, M., Moutiers, G., 2012. In situ time-resolved X-ray near-edge absorption spectroscopy of selenite reduction by siderite. Environ. Sci. Technol. 46, 10820–10826. http://dx.doi.org/10.1021/es301611e.

Bauer, M., Heitmann, T., Macalady, D.L., Blodau, C., 2007. Electron transfer capacities and reaction kinetics of peat dissolved organic matter. Environ. Sci. Technol. 41, 139–145. http://dx.doi.org/10.1021/es061323j.

Behrends, T., van der Veen, I., Hoving, A., Griffioen, J., 2016. First assessment of the pore water composition of Rupel Clay in the Netherlands and the characterisation of its reactive solids. Neth. J. Geosci. 95, 315–335. http://dx.doi.org/10.1017/njg.2016.23.

Bleyen, N., Vasile, M., Mariën, A., Bruggeman, C., Valcke, E., 2016. Assessing the oxidising effect of $NaNO_3$ and $NaNO_2$ from disposed Eurobitum bituminised radioactive waste on the dissolved organic matter in Boom Clay. Appl. Geochem. 68, 29–38. http://dx.doi.org/10.1016/j.apgeochem.2016.03.007.

Borch, T., Kretzschamer, R., Kappler, A., Cappellen, P.V., Ginder-Vogel, M., Voegelin, A., Campbell, K., 2009. Biogeochemical redox processes and their impact on contaminant dynamics. Environ. Sci. Technol. 44, 15–23.

Breynaert, E., Scheinost, A.C., Dom, D., Rossberg, A., Vancluysen, J., Gobechiya, E., Kirschhock, C.E.A., Maes, A., 2010. Reduction of Se(IV) in boom clay: XAS solid phase speciation. Environ. Sci. Technol. 44, 6649–6655. http://dx.doi.org/10.1021/es100569e.

Bruggeman, C., Maes, A., Vancluysen, J., 2007. The interaction of dissolved Boom Clay and Gorleben humic substances with selenium oxyanions (selenite and selenate). Appl. Geochem. 22, 1371–1379. http://dx.doi.org/10.1016/j.apgeochem.2007.03.027.

Bruggeman, C., Maes, N., 2010. Uptake of uranium (VI) by pyrite under Boom Clay conditions: influence of dissolved organic carbon. Environ. Sci. Technol. 44, 4210–4216.

Bruggeman, C., Maes, A., Vancluysen, J., Vandemussele, P., 2005. Selenite reduction in Boom clay: effect of FeS(2), clay minerals and dissolved organic matter. Environ. Pollut. 137, 209–221. http://dx.doi.org/10.1016/j.envpol.2005.02.010.

Caldeira, C.L., Ciminelli, V.S.T., Dias, A., Osseo-Asare, K., 2003. Pyrite oxidation in alkaline solutions: nature of the product layer. Int. J. Miner. Process. 72, 373–386.

http://dx.doi.org/10.1016/S0301-7516(03)00112-1.
Charlet, L., Scheinost, A.C., Tournassat, C., Greneche, J.M., Géhin, A., Fernández-Marti'nez, A., Coudert, S., Tisserand, D., Brendle, J., 2007. Electron transfer at the mineral/water interface: Selenium reduction by ferrous iron sorbed on clay. Geochim. Cosmochim. Acta 71, 5731–5749. http://dx.doi.org/10.1016/j.gca.2007.08.024.
Claff, S.R., Sullivan, L.a., Burton, E.D., Bush, R.T., 2010. A sequential extraction procedure for acid sulfate soils: partitioning of iron. Geoderma 155, 224–230. http://dx.doi.org/10.1016/j.geoderma.2009.12.002.
De Craen, M., Wang, L., Van Geet, M., Moors, H., 2004. Geochemistry of Boom Clay pore water at the Mol site. In: Scientific Report BLG-990. Mol, Belgium, SCK-CEN.
Delécaut, G., 2004. The Geochemical Behaviour of Uranium in the Boom Clay. PhD Dissertation Katholieke Universiteit Leuven, Louvain-La-Neuve Belgium.
Duckworth, O.W., Martin, S.T., 2004. Role of molecular oxygen in the dissolution of siderite and rhodochrosite. Geochim. Cosmochim. Acta 68, 607–621. http://dx.doi.org/10.1016/S0016-7037(00)00464-2.
Gaucher, E., Robelin, C., Matray, J.M., Négrel, G., Gros, Y., Heitz, J.F., Vinsot, A., Rebours, H., Cassagnabère, A., Bouchet, A., 2004. ANDRA underground research laboratory: interpretation of the mineralogical and geochemical data acquired in the Callovian-Oxfordian formation by investigative drilling. Phys. Chem. Earth 29, 55–77. http://dx.doi.org/10.1016/j.pce.2003.11.006.
Gaudette, H.E., 1964. The nature of illite. Clay Clay Miner. 13, 33–48. http://dx.doi.org/10.1346/CCMN.1964.0130105.
Goldhaber, M.B., 1983. Experimental study of metastable sulfur oxyanion formation during pyrite oxidation at pH 6–9 and 30oC. Am. J. Sci. http://dx.doi.org/10.2475/ajs.283.3.193.
Gorski, C.A., Aeschbacher, M., Soltermann, D., Voegelin, A., Baeyens, B., Marques Fernandes, M., Hofstetter, T.B., Sander, M., 2012a. Redox properties of structural Fe in clay minerals. 1. Electrochemical quantification of electron-donating and -accepting capacities of smectites. Environ. Sci. Technol. 46, 9360–9368. http://dx.doi.org/10.1021/es3020138.
Gorski, C.A., Klüpfel, L., Voegelin, A., Sander, M., Hofstetter, T.B., 2012b. Redox properties of structural Fe in clay minerals. 2. Electrochemical and spectroscopic characterization of electron transfer irreversibility in ferruginous smectite, SWa-1. Environ. Sci. Technol. 46, 9369–9377. http://dx.doi.org/10.1021/es302014u.
Gorski, C.A., Klüpfel, L.E., Voegelin, A., Sander, M., Hofstetter, T.B., 2013. Redox properties of structural Fe in clay minerals: 3. Relationships between smectite redox and structural properties. Environ. Sci. Technol. 47, 13477–13485. http://dx.doi.org/10.1021/es403824x.
Gorski, C.A., Sander, M., Aeschbacher, M., Hofstetter, T.B., 2011. Assessing the redox properties of iron-bearing clay minerals using homogeneous electrocatalysis. Appl. Geochem. 26, S191–S193. http://dx.doi.org/10.1016/j.apgeochem.2011.03.101.
Grambow, B., 2016. Geological disposal of radioactive waste in clay. Elements 12, 239–245. http://dx.doi.org/10.2113/gselements.12.4.239.
Griffioen, J., Klaver, G., Westerhoff, W.E., 2016. The mineralogy of suspended matter, fresh and Cenozoic sediments in the fluvio-deltaic Rhine–Meuse–Scheldt–Ems area, the Netherlands: an overview and review. Neth. J. Geosci. 95, 23–107. http://dx.doi.org/10.1017/njg.2015.32.
Hamilton, I.C., Woods, R., 1981. An investigation of surface oxidation of pyrite and pyrrhotite by linear potential sweep voltammetry. J. Electroanal. Chem. Interfacial Electrochem. 118, 327–343. http://dx.doi.org/10.1016/S0022-0728(81)80551-7.
Heron, G., Christensen, T.H., 1995. Impact of sediment-bound iron on redox buffering in a landfill leachate polluted aquifer (Vejen, Denmark). Environ. Sci. Technol. 29, 187–192. http://dx.doi.org/10.1021/es00001a024.
Heron, G., Christensen, T.H., Tjell, J.C., 1994. Oxidation capacity of aquifer sediments. Environ. Sci. Technol. 28, 153–158. http://dx.doi.org/10.1021/es00050a021.
Higgo, J.J.W., 1987. Clay as a barrier to radionuclide migration. Prog. Nucl. Energy 19, 173–207. http://dx.doi.org/10.1016/0149-1970(87)90015-1.
Holmes, P.R., Crundwell, K., 2000. The kinetics of the oxidation of pyrite by ferric ions and dissolved oxygen: An electrochemical study. Geochim. Cosmochim. Acta 64, 263–274.
Honty, M., De Craen, M., 2012. Boom Clay mineralogy – qualitative and quantitative aspects. In: External Report of the Belgian Nuclear Research Centre, Mol, Belgium. SCK•CEN: CO-90-08-2214-00 NIRAS/ONDRAF: CCHO 2009-0940000, .
IAEA, 2003. Scientific and Technical Basis for the Geological Disposal of Radioactive Wastes. International Atomic Energy (IAEA), Vienna, Austria.
IAEA, 2013. Characterization of Swelling Clays as Components of the Engineered Barrier System for Geological Repositories Results of an IAEA Coordinated Research. IAEA-TECDOC-1718. Project 2002–2007. International Atomic Energy (IAEA), Vienna, Austria.
Jaisi, D.P., Dong, H., Liu, C., 2007. Influence of biogenic Fe(II) on the extent of microbial reduction of Fe(III) in clay minerals nontronite, illite, and chlorite. Geochim. Cosmochim. Acta 71, 1145–1158. http://dx.doi.org/10.1016/j.gca.2006.11.027.
Jaisi, D.P., Dong, H., Plymale, A.E., Fredrickson, J.K., Zachara, J.M., Heald, S., Liu, C., 2009. Reduction and long-term immobilization of technetium by Fe(II) associated with clay mineral nontronite. Chem. Geol. 264, 127–138. http://dx.doi.org/10.1016/j.chemgeo.2009.02.018.
Johnston, J.H., Cardile, C.M., 1987. Iron Substitution in Montmorillonite, Illite, and Glauconite by 57Fe Mossbauer Spectroscopy. 35. pp. 170–176.
Kelsall, G.H., Yin, Q., Vaughan, D.J., England, K.E.R., Brandon, N.P., 1999. Electrochemical oxidation of pyrite (FeS_2) in aqueous electrolytes. J. Electroanal. Chem. 471, 116–125.
Kim, J.D., Yee, N., Nanda, V., Falkowski, P.G., 2013. Anoxic photochemical oxidation of siderite generates molecular hydrogen and iron oxides. Proc. Natl. Acad. Sci. U. S. A. 110, 10073–10077. http://dx.doi.org/10.1073/pnas.1308958110.
Klein, A.R., Silvester, E., Hogan, C.F., 2014. Mediated electron transfer between FeII adsorbed onto hydrous ferric oxide and a working electrode. Environ. Sci. Technol. 48, 10835–10842.
Klüpfel, L., Piepenbrock, A., Kappler, A., Sander, M., 2014. Humic substances as fully regenerable electron acceptors in recurrently anoxic environments. Nat. Geosci. 7, 195–200. http://dx.doi.org/10.1038/NGEO2084.
Koenen, M., Griffioen, J., 2016. Characterisation of the geochemical heterogeneity of the Rupel Clay Member in the Netherlands. Neth. J. Geosci. 95, 269–281. http://dx.doi.org/10.1017/njg.2016.6.
Kostka, J., Wu, J., Nealson, K., Stucki, J., 1999. The impact of structural Fe (III) reduction by bacteria on the surface chemistry of smectite clay minerals. Geochim. Cosmochim. Acta 63, 3705–3713. http://dx.doi.org/10.1016/S0016-7037(99)00199-4.
Langmuir, D., 1997. Aqueous Environmental Geochemistry. Prentice Hall, Upper Saddle River, N.J.
Lau, M.P., Sander, M., Gelbrecht, J., Hupfer, M., 2015. Solid phases as important electron acceptors in freshwater organic sediments. Biogeochemistry 123, 49–61. http://dx.doi.org/10.1007/s10533-014-0052-5.
Lau, M.P., Sander, M., Gelbrecht, J., Hupfer, M., 2016. Spatiotemporal redox dynamics in a freshwater lake sediment under alternating oxygen availabilities: combined analyses of dissolved and particulate electron acceptors. Environ. Chem. 13 (A–L). http://dx.doi.org/10.1071/EN15217.
Lee, S.Y., Tank, R.W., 1985. Role of clays in the disposal of nuclear waste: a review. Appl. Clay Sci. 1, 145–162. http://dx.doi.org/10.1016/0169-1317(85)90570-8.
Liu, D., Dong, H., Bishop, M.E., Zhang, J., Wang, H., Xie, S., Wang, S., Huang, L., Eberl, D.D., 2012. Microbial reduction of structural iron in interstratified illite-smectite minerals by a sulfate-reducing bacterium. Geobiology 10, 150–162. http://dx.doi.org/10.1111/j.1472-4669.2011.00307.x.
Long, H., Dixon, D.G., 2004. Pressure oxidation of pyrite in sulfuric acid media: a kinetic study. Hydrometallurgy 73, 335–349. http://dx.doi.org/10.1016/j.hydromet.2003.07.010.
Luan, F., Gorski, C.A., Burgos, W.D., 2014. Thermodynamic controls on the microbial reduction of iron-bearing nontronite and uranium. Environ. Sci. Technol. 48, 2750–2758. http://dx.doi.org/10.1021/es404885e.
Malla, P.B., Robert, M., Douglas, L.A., Tessier, D., Komarneni, S., 1993. Charge heterogeneity and nanostructure of 2:1 layer silicates by high-resolution transmission electron microscopy. Clay Clay Miner. 41, 412–422. http://dx.doi.org/10.1346/CCMN.1993.0410402.
Moses, C.O., Herman, J.S., 1991. Pyrite oxidation at circumneutral pH. Geochim. Cosmochim. Acta 55, 471–482.
Moses, C., Nordstrom, D.K., Herman, J.S., Mills, A.L., 1987. Aqueous pyrite oxidation by dissolved oxygen and by ferric iron. Geochim. Cosmochim. Acta 51, 1561–1571.
Murad, E., Wagner, U., 1994. The Mossbauer spectrum of illite. Clay Miner. 29, 1–10.
Mycroft, J.R., Bancroft, G.M., McIntyre, N.S., Lorimer, J.W., Hill, I.R., 1990. Detection of sulphur and polysulphides on electrochemically oxidized pyrite surfaces by X-ray photoelectron spectroscopy and Raman spectroscopy. J. Electroanal. Chem. 292, 139–152. http://dx.doi.org/10.1016/0022-0728(90)87332-E.
Neumann, A., Petit, S., Hofstetter, T.B., 2011a. Evaluation of redox-active iron sites in smectites using middle and near infrared spectroscopy. Geochim. Cosmochim. Acta 75, 2336–2355. http://dx.doi.org/10.1016/j.gca.2011.02.009.
Neumann, A., Sander, M., Hofstetter, T.B., 2011b. Redox properties of structural Fe in smectite clay minerals. In: Tratnyek, P. et al. (Ed.), Aquatic redox chemistry. ACS Symposium Series American Chemical Society, Washington, DC, pp. 361–379.
Parker, A., Rae, J.E. (Eds.), 1998. Environmental Interactions of Clays: Clays and the Environment. 2 Springer-Verlag, Berlin, Germany.
Pedersen, J.K., Bjerg, P.L., Christensen, T.H., 1991. Correlation of nitrate profiles with groundwater and sediment characteristics in a shallow sandy aquifer. J. Hydrol. 124, 263–277. http://dx.doi.org/10.1016/0022-1694(91)90018-D.
Rakshit, S., Matocha, C.J., Coyne, M.S., 2008. Nitrite reduction by siderite. Soil Sci. Soc. Am. J. 72, 1070. http://dx.doi.org/10.2136/sssaj2007.0296.
Reitz, A., Pfeifer, K., De Lange, G.J., Klump, J., 2004. Biogenic barium and the detrital Ba/Al ratio: a comparison of their direct and indirect determination. Mar. Geol. 204, 289–300. http://dx.doi.org/10.1016/S0025-3227(04)00004-0.
Ribeiro, F.R., Fabris, J.D., Kostka, J.E., Komadel, P., Stucki, J.W., 2009. Comparisons of structural iron reduction in smectites by bacteria and dithionite: II. A variable-temperature Mössbauer spectroscopic study of Garfield nontronite. Pure Appl. Chem. 81, 1499–1509. http://dx.doi.org/10.1351/PAC-CON-08-11-16.
Sander, M., Hofstetter, T.B., Gorski, C.A., 2015. Electrochemical analyses of redox-active iron minerals: a review of nonmediated and mediated approaches. Environ. Sci. Technol. 49, 5862–5878. http://dx.doi.org/10.1021/acs.est.5b00006.
Sasaki, K., Tsunekawa, M., Ohtsuka, T., Konno, H., 1998. The role of sulfur-oxidizing bacteria Thiobacillus thiooxidans in pyrite weathering. Colloids Surf. A Physicochem. Eng. Asp. 133, 269–278. http://dx.doi.org/10.1016/S0927-7757(97)00200-8.
Scheinost, A.C., Charlet, L., 2008. Selenite reduction by mackinawite, magnetite and siderite: XAS characterization of nanosized redox products. Environ. Sci. Technol. 42, 1984–1989.
Seabaugh, J.L., Dong, H., Kukkadapu, R.K., Eberl, D.D., Morton, J.P., Kim, J., 2006. Microbial reduction of Fe(III) in the Fifthian and Muloorina illites: contrasting extents and rates of bioreduction. Clay Clay Miner. 54, 67–79. http://dx.doi.org/10.1346/CCMN.2006.0540109.
Stipp, S.L.S., 1999. Toward a conceptual model of the calcite surface: hydration, hydrolysis, and surface potential. Geochim. Cosmochim. Acta 63, 3121–3131. http://dx.doi.org/10.1016/S0016-7037(99)00239-2.
Stucki, J.W., 2011. A review of the effects of iron redox cycles on smectite properties. Compt. Rendus Geosci. 343, 199–209.
Taylor, R.W., Shen, S., Bleam, W.F., Tu, S.I., 2000. Chromate removal by dithionite-reduced clays: evidence from direct X-ray adsorption near edge spectroscopy (xanes) of chromate reduction at clay surfaces. Clay Clay Miner. 48, 648–654. http://dx.doi.

org/10.1346/CCMN.2000.0480606.
Todd, E.C., Sherman, D.M., 2003. Surface oxidation of chalcocite (Cu_2S) under aqueous (pH = 2–11) and ambient atmospheric conditions: mineralogy from Cu L- and OK-edge X-ray absorption spectroscopy. Am. Mineral. 88, 1652–1656.
Turcotte, S.B., Benner, R.E., Riley, A.M., Li, J., Wadsworth, M.E., Bodily, D.M., 1993. Surface analysis of electrochemically using Raman spectroscopy oxidized metal sulfides. J. Electroanal. Chem. 347, 195–205. http://dx.doi.org/10.1016/0022-0728(93)80088-Y.
Turner, B.D., Binning, P.J., Turner, B.D., Yang, M., Hashimoto, T., Hoshi, N., Myoga, H., Poonam, M., Suja, G., Dhiraj, M., 2014. Fluoride removal by calcite: evidence for fluorite precipitation and surface adsorption fluoride removal by calcite: evidence for fluorite precipitation and surface adsorption. Water Res. 33, 3395–3402. http://dx.doi.org/10.1021/es0505090.
Van der Perk, M., 2006. Soil and Water Contamination, From Molecular to Catchment Scale. Taylor and Francis Ltd.
Viollier, E., Inglett, P.W., Hunter, K., Roychoudhury, A.N., Van Capelle, P., 2000. The ferrozine method revisited: Fe(II)/Fe(III) determination in natural waters. Appl. Geochem. 15, 785–790.
Wade, M.L., Agresti, D.G., Wdowiak, T.J., Armendarez, L.P., Farmer, J.D., 1999. A Mössbauer investigation of iron-rich terrestrial hydrothermal vent systems: lessons for Mars exploration. J. Geophys. Res. Planets 104, 8489–8517.
Walpen, N., Schroth, M.H., Sander, M., 2016. Quantification of phenolic antioxidant moieties in dissolved organic matter by flow-injection analysis with electrochemical detection. Environ. Sci. Technol. 50, 6423–6432. http://dx.doi.org/10.1021/acs.est.6b01120.
Walter, L.M., Morse, J.W., 1984. Reactive surface area of skeletal carbonates during dissolution; effect of grain size. J. Sediment. Res. 54, 1081–1090. http://dx.doi.org/10.1306/212F8562-2B24-11D7-8648000102C1865D.
Wersin, P., Leupin, O.X., Mettler, S., Gaucher, E.C., Mäder, U., De Canniere, P., Vinsot, A., Gäbler, H.E., Kunimaro, T., Kiho, K., Eichinger, L., 2011. Biogeochemical processes in a clay formation in situ experiment: part a – overview, experimental design and water data of an experiment in the Opalinus Clay at the Mont Terri Underground Research Laboratory, Switzerland. Appl. Geochem. 26, 931–953.
Xu, Y., Schoonen, M.A.A., 1995. The stability of thiosulfate in the presence of pyrite in low-temperature aqueous solutions. Geochim. Cosmochim. Acta 59, 4605–4622. http://dx.doi.org/10.1016/0016-7037(95)00331-2.
Zeelmaekers, E., 2011. Computerized Qualitative and Quantitative Clay Mineralogy: Introduction and Application to Known Geological Cases. Katholieke Universiteit Leuven.